In vivo cardiac phase response curve elucidates human respiratory heart rate variability

Published in: *Nature Communications*, 4:2418 (2013); doi: 10.1038/ncomms3418

Björn Kralemann[1], Matthias Frühwirth[2], Arkady Pikovsky[3], Michael Rosenblum[3], Thomas Kenner[4], Jochen Schaefer[5], and Maximilian Moser[2,4]

[1]Institut für Pädagogik, Christian-Albrechts-Universität zu Kiel, Olshausenstr. 75, 24118 Kiel, Germany

[2]Human Research Institute of Health Technology and Prevention Research, Franz Pichler Str. 30, A-8160 Weiz, Austria

[3]Department of Physics and Astronomy, University of Potsdam, Karl-Liebknecht-Str. 24/25, 14476 Potsdam-Golm, Germany

[4]Institute of Physiology, Medical University, Harrachgasse 21/5, A-8010 Graz, Austria

[5]International Institute for Theoretical Cardiology, Schilkseer Strasse 221, 24159 Kiel, Germany

Recovering interaction of endogenous rhythms from observations is challenging, especially if a mathematical model explaining the behaviour of the system is unknown. The decisive information for successful reconstruction of the dynamics is the sensitivity of an oscillator to external influences, which is quantified by its phase response curve. Here we present a technique that allows the extraction of the phase response curve from a non-invasive observation of a system consisting of two interacting oscillators – in this case heartbeat and respiration – in its natural environment and under free-running conditions. We use this method to obtain the phase coupling functions describing cardio-respiratory interactions and the phase response curve of 17 healthy humans. We show for the first time at which phase the cardiac beat is susceptible to respiratory drive and extract the respiratory-related component of heart rate variability. This non-invasive method for the determination of phase response curves of coupled oscillators may find application in many scientific disciplines.

Since observation of respiratory-related variation of the heart rate by S. Hales in 1733 and its first registration by C. Ludwig in 1847 [1], cardio-respiratory interaction (CRI) remains a challenging physiological phenomenon. Respiratory sinus arrhythmia as a component of heart rate variability has become important in many medical fields as a diagnostically and prognostically meaningful indicator of vagal activity. In a more general context, understanding interaction of oscillatory systems is a key problem for many areas of research, especially in life sciences, where rhythmical activity is both abundant and important. Many biological (sub)systems exhibit endogenous rhythms; quantification of their interaction with the environment is relevant for getting insight into the orchestration of organismic processes, the dynamics of neuronal ensembles, determination of brain connectivity, study of robustness of circadian rhythms, etc. [2–6]. A key feature determining the interaction properties is the ability of an oscillator to respond, by shifting its phase, to an external perturbation; this feature is often quantified in terms of phase response curves (PRC), which describe both reaction to a single pulse perturbation and to a continuous force, resulting in a continuous phase shift in the latter case [2, 3, 7, 8]. This approach is used in neuroscience [9–11], cardio-respiratory physiology [12–17], and chronobiology [18, 19], to name just a few. A traditional experimental approach to obtain the PRC implies that the oscillator (e.g., a neuron) is isolated from the environment (e.g., from other neurons which normally interact with it) and is repeatedly perturbed by (weak) short pulses [20]. PRC is then defined as the phase shift evoked by the pulse; this shift is expressed as a function of the fraction of the oscillation period, at which the pulse is applied. The aim of this Communication is twofold: we present a new framework which allows us to reveal the PRC without isolating the system from its environment and without adding any specially designed perturbation, but from simple observation of the system and of the environment under free-running conditions, and determine the PRC of human heartbeat *in vivo*.

PRC is one of the basic concepts of nonlinear science [2, 3, 7, 8], universally applicable to endogenous, self-sustained oscillators (and clusters of oscillators [21, 22]) of various nature: physical, chemical, biological, etc. The starting point here is a parametrisation of the state of an isolated system with well-pronounced rhythmicity, e.g. of an atrial pacemaker cell, by the phase φ. This uniformly growing variable measures the fraction of the time within

one undisturbed cycle. An (not too strong) interaction with another endogenous oscillator can be characterised by the coupled dynamics of two phases φ_1, φ_2 [7]:

$$\begin{aligned} \dot{\varphi}_1 &= Q_1(\varphi_1, \varphi_2) = \omega_1 + q_1(\varphi_1, \varphi_2) \ , \\ \dot{\varphi}_2 &= Q_2(\varphi_1, \varphi_2) = \omega_2 + q_2(\varphi_2, \varphi_1) \ , \end{aligned} \tag{1}$$

where $\omega_{1,2}$ are natural, autonomous frequencies and $q_{1,2}$ are called the coupling (interaction) functions. (Following the tradition of the physics literature, we understand coupling as the presence of an interaction between the oscillators, whereas in the biological literature coupling is often understood as a correlation between their outputs, e.g. due to phase locking, cf. [23–25].) Equations (1) describe the ideal case when the two interacting oscillators are noise-free and are isolated from the rest of the world. If one goes beyond this ideal case, then the right hand side of Eqs. (1) contains additional terms, not related to the coupling, cf. Eq. (3) below. We stress that here we exploit the general concept of the phase from the dynamical systems theory. It characterizes relative accelerations/decelerations at different stages of the cycle; physiological (biological, physical, etc.) interpretation of phase values requires a separate consideration for any particular system.

Theory [7] suggests that for weak interaction the coupling functions in typical cases can be written as

$$q_1(\varphi_1, \varphi_2) = Z_1(\varphi_1) I_2(\varphi_2) \ , \tag{2}$$

where $Z_1(\varphi_1)$ is the PRC of the first oscillator and $I_2(\varphi_2)$ is the forcing with which the oscillator 2 acts on 1, and similarly for $q_2 = Z_2(\varphi_2) I_1(\varphi_1)$. However, even if the governing equations for the interacting systems are known (like for many physical and engineering systems), the derivation of the phase model (1) and of the PRC represents a complicated theoretical problem. In this Communication we develop a novel approach, based on data analysis of free running systems and demonstrate how the functions q, Z, I can be obtained non-invasively, from observations of the coupled oscillatory systems in their natural environment.

The advantage of using the phase model is its universal form. However, one cannot measure the phases directly; in fact only the time series of one or several observables of each oscillator are available. Typically, the phase is estimated from these time series [26–29], but these estimates naturally depend on the observables and their processing. On the contrary, in the theory leading to Eqs. (1), the phase is introduced in a unique way, as the variable that uniformly parametrises the motion along the closed attractive curve in the state space of the dynamical system, i.e. along the limit cycle. The gap between the theory and data-based model reconstruction can be bridged by means of the transformation of the initial phase estimate, called protophase, to the true phase, consistent with the theoretical definition [27]. This transformation ensures invariance of the model reconstruction and, hence, of the PRC determination for a large class of observables. We apply this approach for the first time to analyse the CRI in healthy humans, where we consider the heartbeat and the respiratory cycles as outputs of coupled oscillatory systems approximately obeying the description (1). From the observations of the electrocardiogram and arterial pulse and from the measurements of the respiration we first determine the true phases of these oscillators, then find the interaction function q, and finally determine the PRC Z and the forcing I.

Human CRI has been studied for decades [23–25, 30–33]. It has gained increased interest due to extensive application of ideas from nonlinear dynamics and information theory to medical problems, e.g. to the use of heart rate variability (HRV) as an indicator of autonomic activity. As a result, many aspects of cardio-respiratory coordination, like the degree of locking and the directionality of interaction, have been investigated [26, 28, 29, 34–40].

Here, exploiting the invariant approach and the novel technique for the phase estimation of complex signals, we perform the evaluation of the coupling function and its decomposition into the PRC of the intact human heart and the respiratory forcing. Based on this we quantify the respiratory-related component of the heart rate variability. This complete, from the viewpoint of the nonlinear dynamics theory, description of the phase dynamics of the CRI is promising for quantification of HRV.

RESULTS

Coupling function and PRC from passive observation. First we outline our framework (Fig. 1) for the coupling function reconstruction (cf. [27, 40, 41]) and the PRC determination from data. We emphasise the novel aspects of the procedure, whereas the details are described in *Methods* and *Supplementary Information*.

The first step is to obtain high-resolution recordings of observables from two systems – one observable for the respiratory system and two different observables for the cardio-vascular one: the ECG and the arterial pulse.

The second step is parametrising the signal by an angle variable θ that grows monotonically in time and gains 2π at each cycle. It is important that this variable, called protophase [27], is unambiguously determined from the state of the oscillatory system. For complex waveforms like the ECG signal the construction of the protophase is highly non-trivial. Here we use a novel three-step technique: first we define 6 marker events within each cardiac cycle and introduce a preliminary cyclic variable from the conditions that it gains 2π between two R-peaks and linearly increases with time between the events. Next, we use this initial estimate to construct the average cycle and define a new, improved continuous protophase on it;

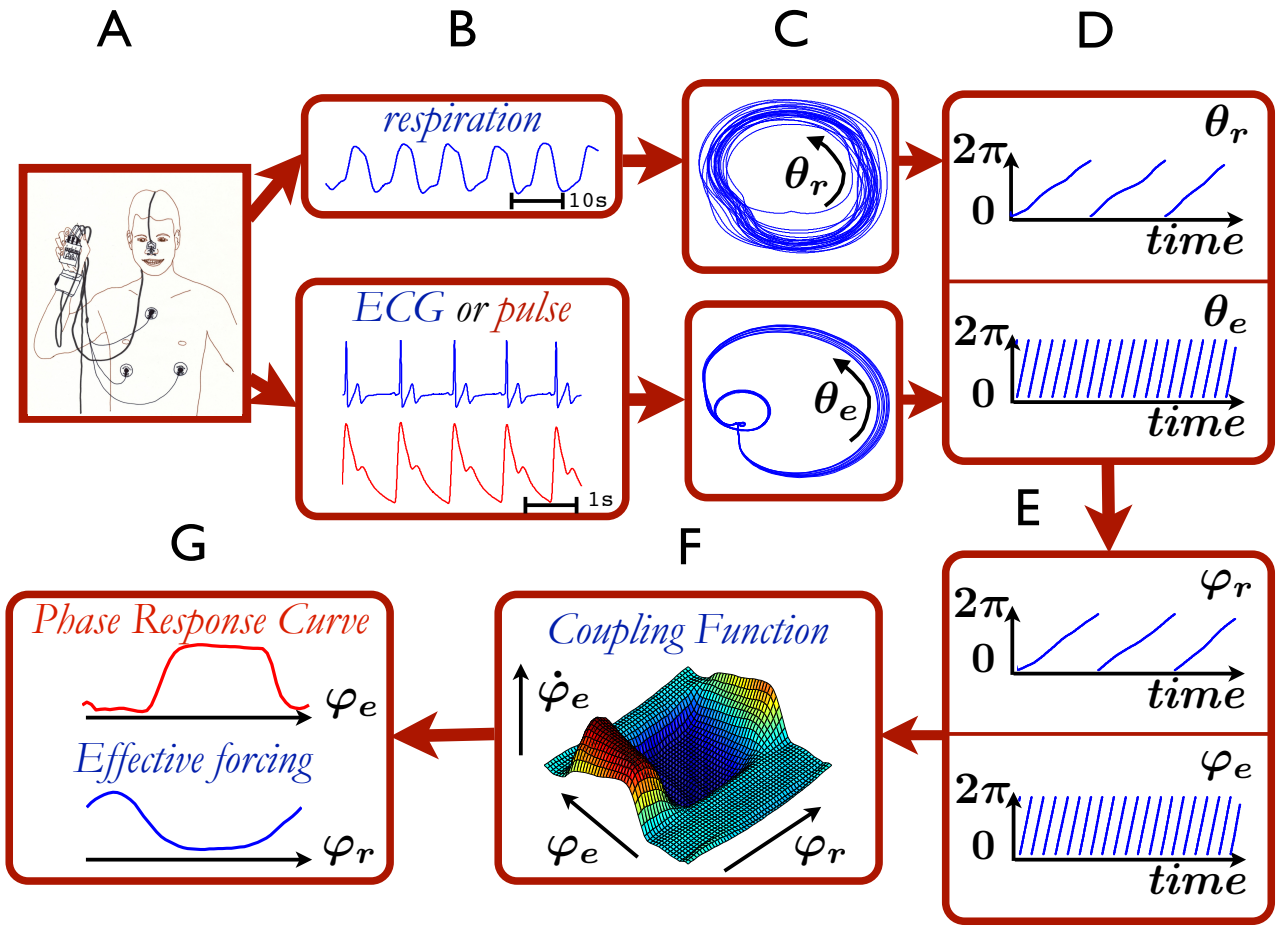

FIG. 1. Phase response curve from non-invasive observation: scheme of the approach. (A-B): The respiratory signal, the electrocardiogram, and the arterial pulse are simultaneously recorded from subjects in resting state. (C-D): From these scalar signals, by virtue of a proper two-dimensional embedding, the protophases $\theta_{\rm r}$, $\theta_{\rm e}$, and $\theta_{\rm p}$ are obtained and transformed to the phases $\varphi_{\rm r}$, $\varphi_{\rm e}$, and $\varphi_{\rm p}$, shown in E. (In this schematic representation the difference between $\theta_{\rm e}$ and $\varphi_{\rm e}$ is not seen). (F): The coupling (interaction) function describing the effect of respiration on heart dynamics is reconstructed in an invariant way. (G): The coupling function is decomposed into the phase response curve PRC and the respiratory forcing.

finally we assign the protophases to all points of the state plane trajectory by projecting them onto the average cycle. The protophase for the arterial pulse is obtained in a similar way, using 3 markers.

The next step is to transform the protophases θ to phases φ, to match the underlying condition of Eq. (1) that the phase of an autonomous system grows uniformly in time. In this way an arbitrary protophase is mapped on to the uniquely defined phase; moreover the transformation $\theta \to \varphi$ is fully invertible and does not contain any filtering. Practically, it is performed by means of the probability distribution of θ which is obtained by virtue of a kernel function [27, 42].

Having two time series of the phases $\varphi_{1,2}$, we represent their dynamics according to Eqs. (1), via reconstructing the right hand sides of Eqs. (1) by virtue of two-dimensional kernel functions. We denote the phases from the ECG, the arterial pulse, and the respiratory signal as $\varphi_{\rm e}$, $\varphi_{\rm p}$, and $\varphi_{\rm r}$, respectively. We reconstruct only the phase dynamics of the cardiac system, i.e. only one of the Eq. (1); in the new notations it reads

$$\begin{aligned} \dot{\varphi}_{\rm e} &= \omega_{\rm e} + q_{\rm e}(\varphi_{\rm e},\varphi_{\rm r}) + \xi_{\rm e} = Q_{\rm e}(\varphi_{\rm e},\varphi_{\rm r}) + \xi_{\rm e} \quad \text{or} \\ \dot{\varphi}_{\rm p} &= \omega_{\rm p} + q_{\rm p}(\varphi_{\rm p},\varphi_{\rm r}) + \xi_{\rm p} = Q_{\rm p}(\varphi_{\rm p},\varphi_{\rm r}) + \xi_{\rm p} \, . \end{aligned} \tag{3}$$

The residues of fitting $\xi_{\rm e,p}(t)$ include noise and effects of non-observed physiological rhythms other than respiration, i.e. $\xi_{\rm e,p}$ describes all perturbations to the heart dynamics which do not depend on $\varphi_{\rm r}$. As the ECG and the arterial pulse represent two different observables of the cardiac system, ideally functions $Q_{\rm e}(\varphi_{\rm e},\varphi_{\rm r})$, $Q_{\rm p}(\varphi_{\rm p},\varphi_{\rm r})$ should coincide. In practice they are very similar in shape (Fig. 2), which confirms the reliability of our approach and its invariance with respect to the used observables, due to the $\theta \to \varphi$ transformation.

The last stage is an optimal decomposition $Q_{\rm e,p}(\varphi_{\rm e,p},\varphi_{\rm r}) = \omega_{\rm e,p} + Z(\varphi_{\rm e,p})I(\varphi_{\rm r}) + \beta(\varphi_{\rm e,p},\varphi_{\rm r})$,

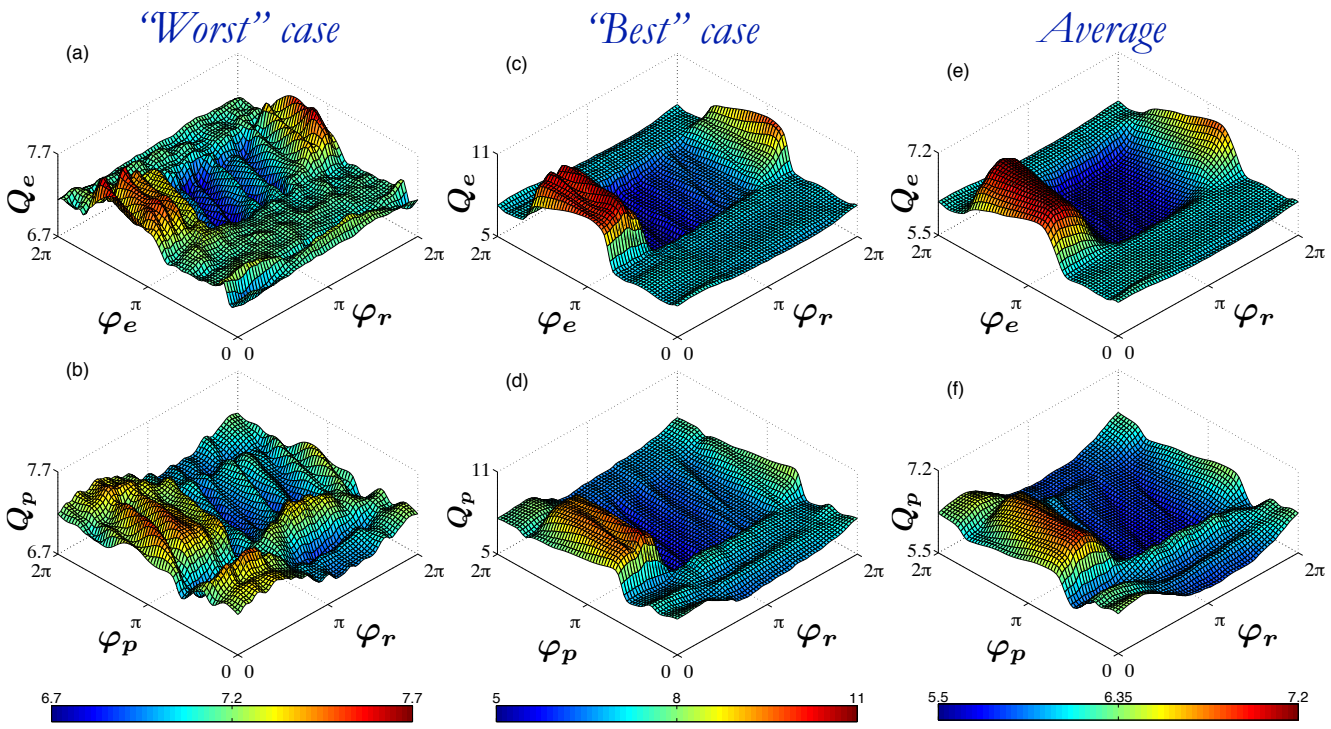

FIG. 2. Coupling functions for the human cardio-respiratory system. The reconstructed functions provide the dependence of the instantaneous cardiac frequency, measured in radians per second, on the cardiac and respiratory phases. Red regions mean higher frequencies (acceleration) while blue regions correspond to lower frequencies (deceleration). Functions $Q_{\rm e}(\varphi_{\rm e},\varphi_{\rm r})$ (a,c,e) are obtained from the ECG and the respiration, whereas functions $Q_{\rm p}(\varphi_{\rm p},\varphi_{\rm r})$ (b,d,f) are computed from arterial pulse and respiration. Using these two very different observables for the cardio-vascular system, we nevertheless obtain highly correlated results, as is expected for the invariant approach. The functions for the subject with the lowest correlation between $Q_{\rm e}$ and $Q_{\rm p}$ are shown in (a,b), and for the subject with the highest correlation in (c,d). Panels (e,f) present the averaged (over all measurements for all subjects) coupling functions $Q_{\rm e}$ and $Q_{\rm p}$.

cf. Eq. (2), which minimises the residual error β. We find that the error is relatively small; hence, the resulting functions $Z(\varphi_{\rm e,p})$ and $I(\varphi_{\rm r})$ can be interpreted, according to the theoretical framework, as the PRC and the driving force, respectively.

Coupling function for cardio-respiratory interaction. The intermediate result of our analysis, i.e. the reconstructed coupling functions $Q_{\rm e,p}(\varphi_{\rm e,p},\varphi_{\rm r})$, are illustrated in Fig. 2. Before making the next step, we discuss the robustness of the obtained functions for different test persons and trials. The reliability of the technique is confirmed by large similarity between the coupling functions among the group, with highest similarity for repeated measurements of the same person. To quantify the similarity between the functions obtained in different trials, we use the correlation coefficient ρ, which quantifies similarity of the forms of two functions (independent on their amplitudes), and the difference measure η, see *Methods*, which also reflects difference in the amplitudes (norms), see Fig. 3. We find that the functions have a well pronounced characteristic shape for each of the subjects (Fig. 2e,f): the correlations between $Q_{\rm e}(\varphi_{\rm e},\varphi_{\rm r})$ obtained in different trials with the same subjects are $\rho \gtrsim 0.6$ (with the average ≈ 0.89). Naturally, the correlation between the functions of different subjects is lower, reflecting the interpersonal variability; however, it is high enough, $\rho \gtrsim 0.43$ (average ≈ 0.81), to demonstrate the high similarity of the CRI in our group of subjects. We emphasise that the high similarity of the functions, obtained from such different observables as the ECG and the arterial pulse, as well as practical coincidence of their norms, supports validity of the transformation to the invariant phase.

We have also performed a surrogate data test [43]. First we computed two functions $Q_{\rm e}$ for a subject, for whom data from two trials are available, Fig. 4a,b. Next, we used exactly the same procedure and computed two functions after interchanging the respiration time series from the trials (Fig. 4c,d). These surrogates keep the properties of the processes, but destroy the correlation between them. The functions shown in Fig. 4e,f are obtained by taking the respiration data of other subjects. Ideally, the functions obtained from the surrogate data should be flat, showing no coupling; in practice we observe some low variability due to accidental phase correlations, because we have only 20 to 40 respiratory cycles.

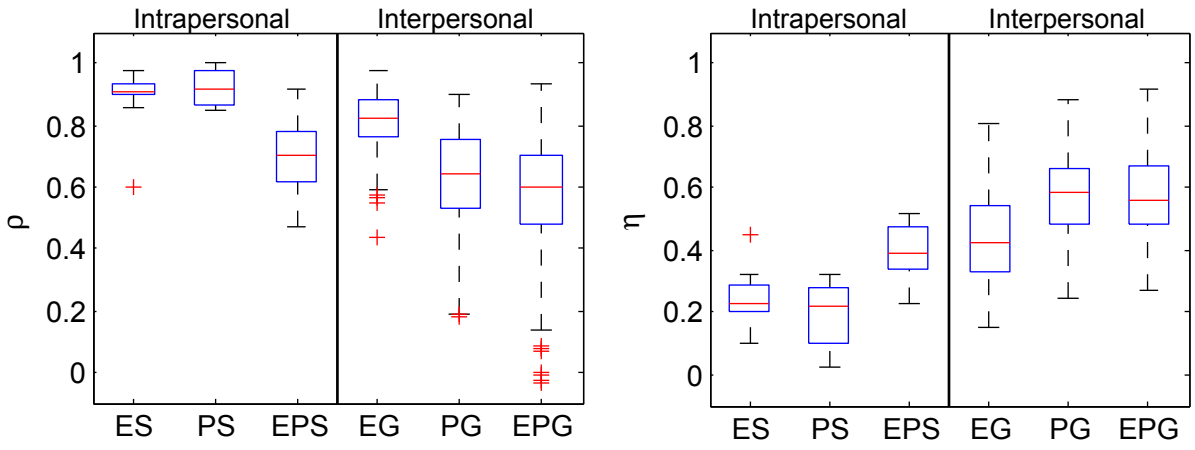

FIG. 3. Similarity measures for the obtained coupling fuctions. Box-whisker plot illustrates the correlation coefficient ρ (a) and the difference measure η (b), for all available pairs of functions (high similarity corresponds to large ρ and small η). ES: similarity between the functions $Q_{\rm e}$ (respiration – ECG) of the same subject, obtained from two trials; it is maximal. EG: similarity between $Q_{\rm e}$ of different subjects in the group demonstrates low interpersonal variability. PS and PG: intra- and interpersonal similarities for $Q_{\rm p}$ (respiration – arterial pulse). EPS and EPG: intra- and interpersonal similarities between $Q_{\rm e}$ and $Q_{\rm p}$. Notice that the correlation can be maximised by computing it for phase-shifted functions; so, e.g., the outlier value in (a) ES, at ≈ 0.6 becomes as high as 0.9. This phase-shift might reflect a variation of internal delays and therefore might have a physiological meaning; however, this issue requires a separate study. The number of cases used for computation of the 6 box plots is (from left to right): 11, 18, 29, 314, 172, 491. (The low border of the box, the red line, and the upper border are the first, second, and third quartiles, respectively. The whisker length is 1.5 times the interquartile range.)

However, the difference measure η between the true and the surrogate functions is approximately one order in the magnitude larger than between the two true functions. We conclude that the detected coupling is not a statistical artefact; however, the surrogate tests do not allow one to check whether all components of the coupling are revealed. The absence of artefacts in the reconstructed function is also supported by numerical tests with artificial ECG signals.

PRC for cardio-respiratory interaction. Final results for the computation of the PRC of the human heartbeat *in vivo* are presented in Fig. 5. Below we restrict ourselves to the coupling functions obtained from the ECG data, since they are of superior quality; the results based on pulse time series are shown in Supplementary Fig. S1. We show both the individual PRCs Z and the forcing functions I for all trials, as well as the group-averaged curves, obtained either by averaging all functions Z and all functions I, or by decomposing the averaged coupling function, shown in Fig. 2e. Because in the decomposition we cannot separately determine the amplitudes of the PRC and of the forcing, only the form of these functions is revealed (in our presentation in Fig. 5 we make the norms of Z and I equal, another option is illustrated in Supplementary Fig. S2). In Fig. 5c,d we also show the relative decomposition errors, they all are in the range between 0.15 and 0.45, with median ≈ 0.265.

The PRC of the heartbeat, which is the main result of this study, clearly exhibits two different domains: in the interval $0.6\pi \lesssim \varphi_{\rm e} \lesssim 1.8\pi$ the phase of the heartbeat can be strongly advanced by respiration forcing, and this susceptible epoch lies between the T and P waves. Another domain ($\varphi_{\rm e} \lesssim 0.6\pi$ and $\varphi_{\rm e} \gtrsim 1.8\pi$) is characterised by nearly zero response, i.e. here the heart is insensitive to respiratory drive. A corresponding interpretation for the respiratory force I follows from Fig. 5b. The functions I are quite close to a sine, but with a typical asymmetry of inspiration/expiration stages. As I changes sign (while Z is positive or close to zero), one can distinguish the different stages of accelerating and decelerating effects of force, and relate them to the stages of inspiration and expiration within the respiration cycle.

Respiratory-related component of the heart rate variability. Description of cardio-respiratory interaction in terms of coupling functions yields a new technique for the quantification of respiratory-related HRV. HRV is one of the central tools of psychophysiology and behavioural medicine [44], and the respiratory component is a significant part of it (see, e.g. [23–25, 45–48]), representing mainly the vagal or parasympathetic part of the autonomic nervous system influences. Having introduced the time-continuous phase of the ECG, we obtain a continuous description of the HRV via the instantaneous frequency $\dot{\varphi}_{\rm e}(t)$, instead of the commonly used discontinuous beat to beat description. Furthermore, using Eqs. (3) we decompose $\dot{\varphi}_{\rm e}(t)$ into two pro-

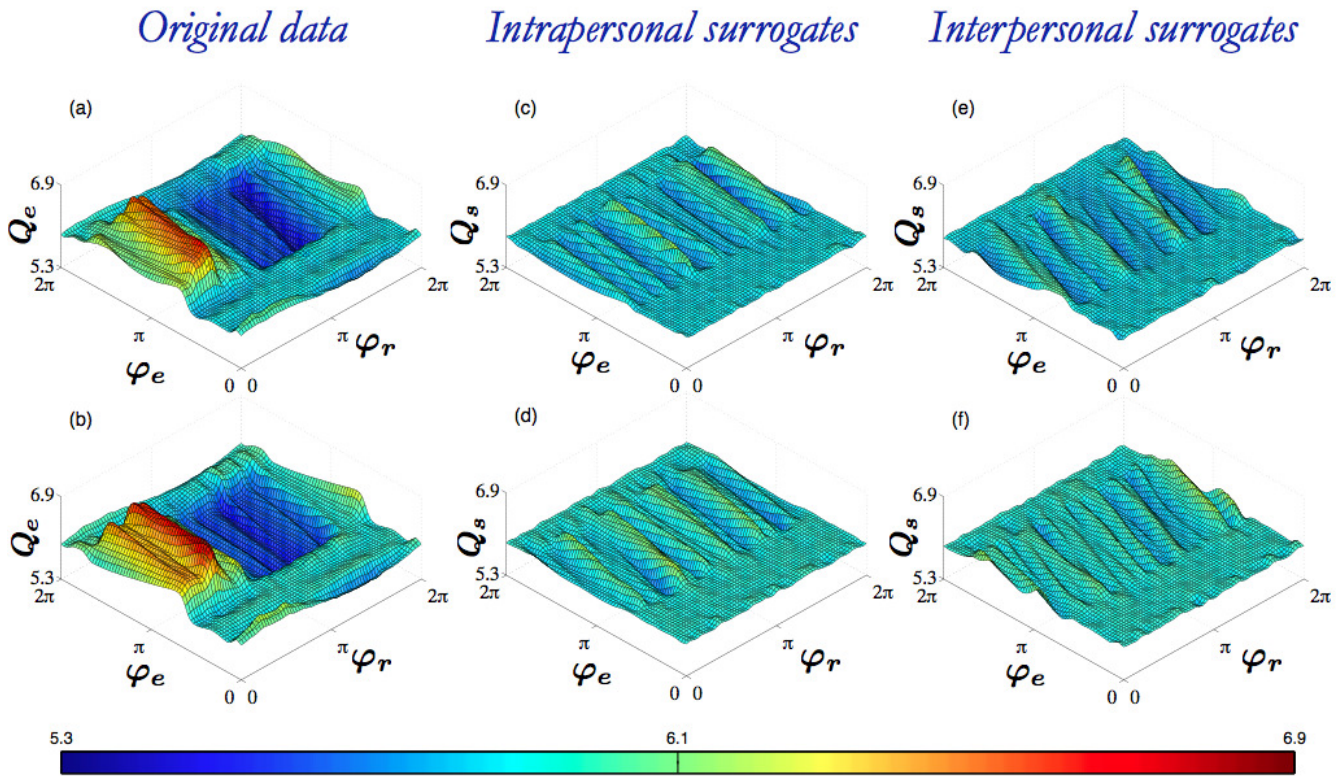

FIG. 4. Surrogate data test. Here we show an essential difference between true functions $Q_{\rm e}$ (here for ECG-respiration) and spurious functions Q_s. (a,b): Coupling functions for two recordings of the same subject (average heart rates are 0.93 Hz and 0.94 Hz, average respiration frequencies are 0.16 Hz and 0.13 Hz). (c,d): Coupling functions obtained after interchanging the respiratory signals from these two measurements. (e,f): Here respiration time series of a different subjects is used (average frequency 0.32). The difference measure, η, between the true functions (a) and (b) is 0.20, while the difference between the true function (a) and the spurious functions (c,e) is 0.81. The difference between (b) and its surrogates (d,f) is 0.80. The difference between the surrogates is in the range from 0.58 to 0.80. The correlation, ρ, between the true functions (a) and (b) is 0.93, while the correlation between the true function (a) and the spurious functions (c,e) is -0.10 and 0.00, respectively. The correlation between (b) and its surrogates (d,f) is 0.13 and 0.25. The absolute value of the correlation between the surrogates is in the range from 0.02 to 0.34.

cesses: the first component, $Q_{\rm e}(\varphi_{\rm e}(t),\varphi_{\rm r}(t))$, reflects the effect of respiration and therefore can be used for characterisation of the respiratory sinus arrhythmia (we use "RSA-HRV" to denote this component), whereas the second component, $\xi_{\rm e}(t)$, is independent of respiration and reflects both intrinsic sources of HRV as well as the effects of other, unobserved, rhythms like baroreflex and/or angiotensin loop rhythms and of random perturbations; we denote it as "non-RSA-HRV". (Noteworthy, in 8 cases the RSA-HRV component is larger that non-RSA-HRV, and in 18 cases it is smaller, indicating, respectively, vagal and sympathetic predominance of the subjects during the measurements.) The quality of this decomposition is confirmed by Fig. 6a: we see that the variances of the components sum up to the full variance of HRV, as is expected for independent components. This result, in addition to opening a new perspective in quantification of the respiratory influence on the heartbeat, provides a confirmation of our approach based on Eq. (3).

To illustrate the decomposition in more detail, we show in Fig. 6(b,c) the power spectra of the original HRV $\dot\varphi$ and of their two components, for two extreme cases, i.e. for maximum and minimum content of RSA-HRV in HRV, measured by the ratio rms(non-RSA-HRV)/rms(HRV). In both cases the main effect on the spectrum is elimination of a peak at the frequency of respiration (around 0.2

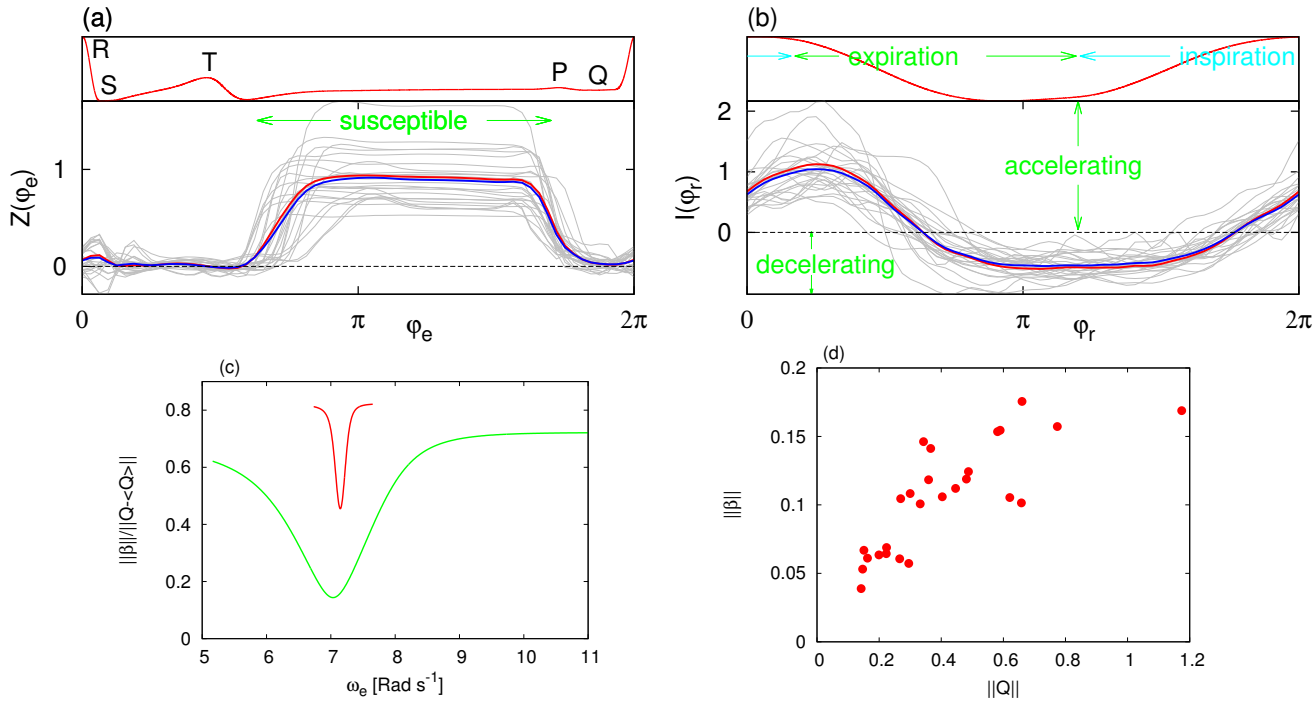

FIG. 5. PRC curves and effective forcing. We show individual PRCs Z (a) and effective forcing I (b) for all ECG-based coupling functions with grey curves. In both panels blue lines show the average over all individual (grey) curves. Red curves are obtained by decomposition of the averaged coupling function, shown in Fig. 2e. Small panel on top of (a) shows for comparison the average ECG cycle as a function of its phase. One can clearly see the interval where PRC is not zero, and, hence, the cardiac system is susceptible for the respiratory perturbation. Small panel on top of (b) shows the average respiratory cycle as a function of the phase, with marked epochs of inspiration and expiration (approximately). Intervals of positive (negative) effective forcing are the intervals where respiration is accelerating (decelerating) the heart rate. Panels (c) and (d) show error of the decomposition $\|\beta\|$, where $||\cdot||$ denotes the norm of the function. In (c) the relative error $\|\beta\|/\|Q-\langle Q\rangle\|$ is shown (for the cases of the largest (red) and of the smallest (green) error) in dependence on the parameter ω_e used in the decomposition procedure; finally the value of ω_e yielding minimal error is chosen. In (d) all errors are presented, demonstrating quality of the decomposition.

Hz). Additionally, some respiration-induced side-bands close to the basic heart frequency are reduced, while the very low frequencies (smaller than 0.1 Hz) remain practically unchanged.

DISCUSSION

We have presented a general framework for determination of PRC from the observations of coupled oscillators under free-running, undisturbed conditions, and have applied it to characterise the respiratory influence on the cardiac cycle in humans. Our reconstruction method is based solely on non-invasively recorded biological data and their analysis, and can be applied to a wide class of coupled self-sustained, endogenous, systems provided the oscillatory observables from both of them are available; the coupling should be not too strong, so that the oscillators remain asynchronous (presence/absence of synchrony can be easily recognized from the data). In our case the decomposition of the coupling function into a product of the PRC and the forcing was successful, which indicates that the interaction between the cardiovascular and the respiratory systems is relatively weak (in the sense of applicability of Eqs. (1)). This allowed us for the first time to obtain the PRC of the heart *in vivo* and without artificial measures like paced breathing. Generally this decomposition may not work, so that the coupling function would be the final stage of the analysis.

For a group of healthy subjects we have determined the functions describing the effective respiratory forcing, I, and the heart PRCs, Z, which, being multiplied, fully quantify the respiratory-related HRV. These functions provide a rather detailed, with a resolution much finer than the cycle length, description of the CRI on the system analysis level, without going into details of background chemical and electrical mechanisms. The functions I are quite close to a sine, but with a typical asymmetry of inspiration/expiration stages, which manifest it-

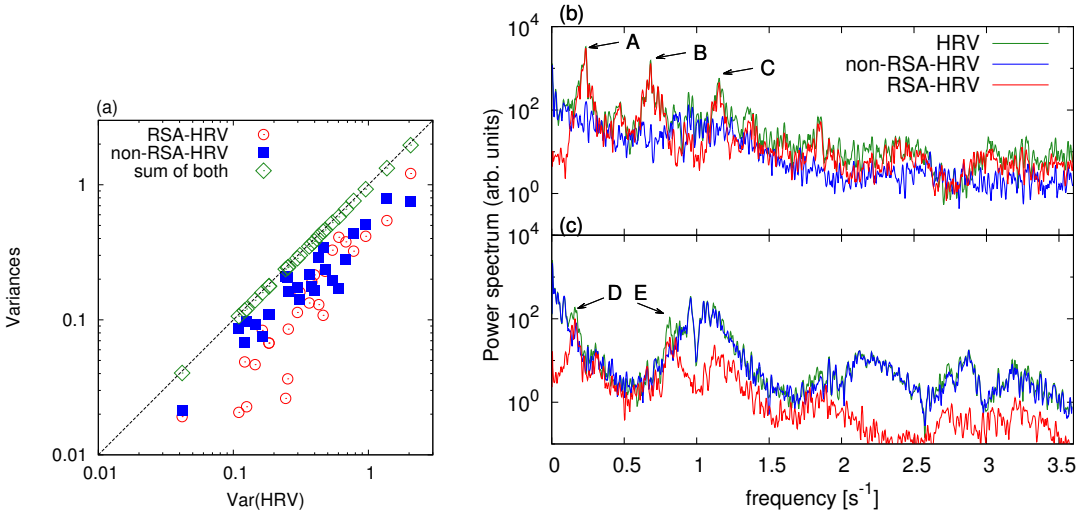

FIG. 6. Extracting the respiratory component of heart rate variability. (a) The variances of the RSA-HRV and non-RSA-HRV signals, as functions of the variance of the original HRV. Green diamonds show the sums Var(RSA-HRV)+Var(non-RSA-HRV), these are nearly equal to Var(HRV) (black dashed line), which means that RSA-HRV and non-RSA-HRV are almost uncorrelated. (b,c) Power spectra of original HRV (green), the RSA-HRV component (red) and of the non-RSA-HRV (blue), in the cases of maximal (b) and minimal (c) relative RSA-HRV component; in (b) $\approx 67\%$ of Var(HRV) is contained in RSA-HRV, indicating vagal predominance, while in (c) only 10% Var(HRV) is in RSA-HRV, indicating sympathetic predominance. In (b) the letters A, B, C mark three respiratory-related peaks, corresponding to average respiratory frequency 0.23 Hz and to side-bands of the heart rate (average value 0.92 Hz), i.e. to 0.92 ± 0.23 Hz. Notice that these peaks (at which the green and red curves practically coincide) are definitely higher than the surrounding, which indicates a strong contribution of RSA-HRV in these frequency bands. Correspondingly, the residual non-RSA-HRV (blue line) is much weaker than HRV and RSA-HRV in these bands. Contrary, in (c) the peaks of RSA-HRV, marked by D (corresponds to average respiratory frequency 0.15 Hz) and E (side-band of the heart rate peak at ≈ 0.82 Hz) are low and the corresponding peaks in HRV only slightly exceed the surrounding, hence, the residual non-RSA-HRV is relatively high.

self in asymmetry of decelerating and accelerating stages of the forcing (Fig. 5b). Contrary, the form of the PRC is highly non-sinusoidal and exhibits an epoch of insusceptibility, $\approx 40\%$ of the cycle length (in phase units), where the PRC is close to zero and the heart is insensitive to forcing (in accordance to the known refractory period of sinoatrial cells [49]). During the epoch of susceptibility the phase of the heart can be influenced by the respiration, to our knowledge mainly by varying vagal control. This epoch coincide with the electrical diastole, i.e. with the interval between T and P waves. This corresponds to the fact that in the second halve of the T-wave the cells of the myocardium recover and become again susceptible to excitation; this epoch is terminated with the next cycle of the sinus node activity, when atrial and ventricular excitation renders the myocardium refractory. The functions I and Z quantify the long known qualitative observation that inspiration accelerates the heart beat, while the expiration slows it down [50] and make it possible for the first time to determine, when these influences take place.

It is well-known [23–25, 45–48, 51, 52] that the phase of respiration influences the peripheral autonomic nervous system's outflow to the heart. However, till now it has never been shown when exactly this happens inside the cardiac cycle. Our results show that this transfer happens when the PRC is highest, i.e. between T and P waves, which is the time of electrical diastole of the heart; they also correctly reveal the existence and timing of the atrial and ventricular refractory phase of the myocardium [49], during which no information transfer takes place. This information is relevant for all models of CRI as well as for clinical problems (in particular because the period of susceptibility is crucial for myocardial fibrillation risk estimation). Our technique of non-invasive determination of refractory and susceptible periods is thus of potentially high medical and clinical relevance, as these periods demonstrate quite an interpersonal variability (see grey lines in Fig. 5a). This information might be used to determine individual myocardial properties relevant for fibrillation. Furthermore, since the duration of electric diastole mainly determines the heart rate [53], the amplitude of PRC can be considered as a measure of adaptability in response to respiratory drive; adaptation of the heart rate is a fundamental prerequisite of the proper functioning of the cardiovascular system. Therefore, quantification of variations of the PRC in amplitude or shape might be helpful for diagnostic of various disease states involving cardiorespiratory dysautonomia [54]. Further statistical studies of PRC dependence on the age, gender, and other factors are needed here.

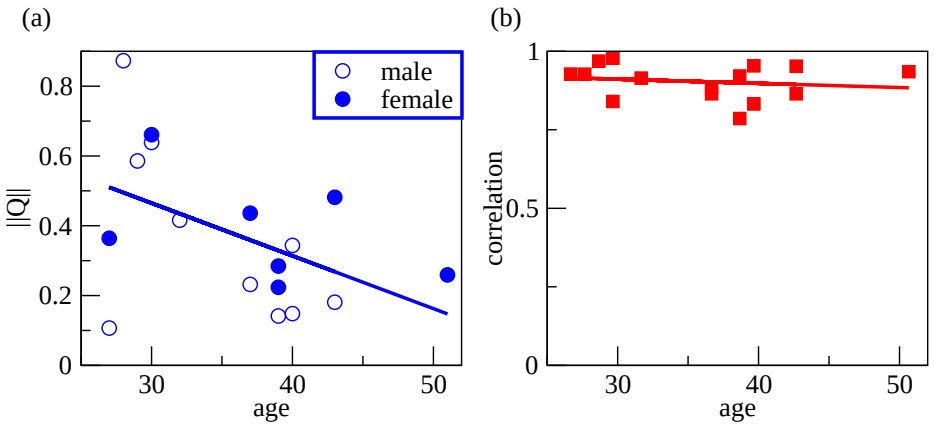

FIG. 7. Characterizing age-dependence of cardio-respiratory interaction. (a) Age-dependence of the norm of the coupling function $\|Q\|$ for male (open circles) and female (filled circles) subjects shows that cardio-respiratory interaction tends to decrease with age (correlation coefficient is -0.48). Each symbol shows the average of norms of all $Q_{\mathrm{e,p}}$ coupling functions available for one subject. (b) The correlation of Q_{e} with the average function shown in Fig. 2e vs the difference of the age and the average age (36 in our group) indicates independence of the shape Q on the age (correlation coefficient is -0.16).

In this paper we mainly concentrated on the reliability and consistency of the developed technique, which is confirmed by similar results obtained from ECG and arterial pulse, which are two essentially different observables of the same system, representing, respectively, electrical and mechanical processes in the heart. A further confirmation of the validity was achieved via a decomposition of the instantaneous frequency time series, which represents the HRV, into two components: the respiratory related and the non-respiratory-related ones, which are found to be statistically independent. This fact indicates that the respiratory-induced part of HRV is correctly captured by our technique. Additionally, this essentially nonlinear decomposition opens new ways for quantification of the RSA and of the HRV, to be compared with other recently suggested decomposition methods based on linear analysis, see e.g. [55, 56]. As the HRV analysis by itself has gained clinical relevance in fields like cardiac risk prognosis, sleep research, and circadian autonomic regulation, we expect that our essentially nonlinear approach will contribute significantly to these studies, allowing one to go beyond a usual linear analysis.

For our group of healthy subjects, the coupling functions and PRCs of the heart have a characteristic, reproducible shape, while the amplitude of these functions varies. This finding makes the approach promising for quantitative studies of possible effects of different factors (age, gender, diseases, drugs, physical load, etc.) on these characteristics of the cardiovascular physiology. To give a flavour of such possibilities, we show in Fig. 7 that the norms $\|Q\|$, and, hence, the RSA-HRV tend to decrease with age, in good correspondence with other studies [57], while the shape of Q does not exhibit an age dependence. However, clinical and physiological applications of cardio-respiratory coupling functions and PRCs require comprehensive statistical studies with different groups of subjects. Another prospective application of the characterisation of CRI through PRC is related to implementation of a proper CRI in computational modelling of cardiac electrophysiology [58].

METHODS

Data. We analysed continuous multichannel recordings from 17 healthy subjects (7 females, 10 males, age between 27 and 51, average 36, see Supplementary Table S1 for details; written informed consent including permission of data use was obtained from all subjects before the measurement). The measurements were done with a custom-made battery-powered device (ChronoCord®, Human Research, Weiz, Austria (www.humanresearch.at), and the University of Applied Sciences FH Joanneum, Kapfenberg, Austria) with Bluetooth® connection to a PC. It is based on a Holter ECG, but was expanded to record four channels, each with the sampling rate of 1 kHz and resolution of 16 bit. The device was equipped with a differential chest-wall ECG, two piezoresistive pressure sensors attached to the wrist of the left and right hands above the arteria radialis close to the location of apophysis radii and yielding arterial pulse signals, and a high-speed thermistor to record the nasal respiratory flow for the respiration signal [59, 60]. For each subject, two recordings of duration 420s were performed in the supine position at rest, with the interval of 12 minutes between the trials; the subjects were quietly and relaxed standing during these breaks. All data have been visually inspected and only time series without large disturbances, e.g. due to motion, swallowing, etc, were analysed (small artefacts

have been manually corrected during preprocessing). Altogether, we have selected and analysed 26 records of respiration – ECG data and 20 records of respiration – arterial pulse data, see Supplementary Table S1. Preprocessing of time series has been performed in the following way: manual correction of artefacts by interpolation (for respiration), smoothing by Savitzky-Golay filter, and elimination of slow baseline fluctuations, see Supplementary Figs. S3, S4, S5.

Phases from data. Protophases of the respiratory signal, $\theta_{\rm r}$, were obtained as angles in the two-dimensional embedding performed with help of the Hilbert Transform (Fig. 8a). Then the protophases were transformed to the phases with the help of the technique of Ref. [27]:

$$\varphi = \theta + 2\sum_{n=1}^{n_F} \mathrm{Im}\left[\frac{S_n}{n}(e^{in\theta}-1)\right] , \qquad (4)$$

where $S_n = n^{-1}\sum_{j=1}^{N} e^{-in\theta(t_j)}$ are the coefficients of the Fourier expansion of the probability distribution density of θ, computed from its time series $\theta(t_j)$, where $j = 1, \ldots, N$. The number of Fourier modes n_F was chosen according to [42]. For such complex signals as ECG, the embedding via the Hilbert Transform does not provide a trajectory with a well-defined centre of rotation (Fig. 8b); therefore we developed the following three-step technique. In the first step, 6 markers are identified within each $PQRST$ complex, corresponding to the maxima of R, T, and P waves and minima of Q, S and of the wave after T (Fig. 8d). The first estimate, Ψ, of the protophase is obtained by means of a linear interpolation between the markers, while the phase of each marker is assigned according to its average position within the cycle; the phase of the R-peak is set to zero. Next, we construct from the ECG the complex analytic signal $z(t)$ by means of the Hilbert Transform, and compute the average cycle (Fig. 8b), parametrised by an angle variable ψ:

$$z_{\rm ac}(\psi) = \sum_{n=0} H_n e^{i\psi} \qquad (5)$$

where H_n are the Fourier coefficients of the function $z(\psi)$:

$$\begin{aligned} H_n =& \frac{1}{\Psi(T)}\int_0^{\Psi(T)} z(\psi)e^{-in\psi}d\psi \\ =& \frac{1}{T}\int_0^T z(t)e^{-in\Psi(t)}\frac{d\Psi(t)}{dt}dt \, . \end{aligned} \qquad (6)$$

As the next step we introduce the protophases $\theta_{\rm e}$, projecting $z(t)$ onto the average cycle with the help of an optimisation strategy, illustrated in Supplementary Figures S6, S7. Finally, the transformation $\theta_{\rm e} \to \varphi_{\rm e}$ was performed according to Eq. (4). The protophases $\theta_{\rm p}$ were obtained via the average cycle technique with 3 markers, see Fig. 8e.

Coupling function reconstruction. For this purpose we use the kernel density estimation. First, for each point in the data set we estimate the derivative of either $\varphi_{\rm e}$ or $\varphi_{\rm p}$ via local polynomial fitting, using the 4th-order Savitzky-Golay filter with the window length 0.008s, which provided a reliable smoothing without losing much information. Next, we fit Eq. (3) on a $n \times n$ grid using the smoothing kernel with the width inverse proportional to n: $K(x,y) = \exp\left[\frac{n}{2\pi}(\cos x + \cos y)\right]$. We compute

$$Q(\varphi_{\rm e,p},\varphi_{\rm r}) = \frac{\sum_{k=1}^{N}\dot{\Phi}_{\rm e,p}(t_k)K(\varphi_{\rm e,p}-\Phi_{\rm e,p}(t_k),\varphi_{\rm r}-\Phi_{\rm r}(t_k))}{\sum_{k=1}^{N}K(\varphi_{\rm e,p}-\Phi_{\rm e,p}(t_k),\varphi_{\rm r}-\Phi_{\rm r}(t_k))} \, . \qquad (7)$$

Here $\varphi_{\rm e,p}$ and $\varphi_{\rm r}$ denote the points on the grid, where the functions $Q_{\rm e,p}$ are estimated, whereas $\Phi_{\rm e,p}$ and $\Phi_{\rm r}$ denote the time series of cardiac and respiratory phases, respectively. We choose $n = 64$ which yields ≈ 100 observation points per grid cell.

Similarity between the functions is quantified by the correlation coefficient $\rho = \langle\tilde{Q}_1\tilde{Q}_2\rangle\|\tilde{Q}_1\|^{-1}\|\tilde{Q}_2\|^{-1}$, which measures similarity of the forms of two functions (independently of their amplitudes), and by the difference measure $\eta = \|\tilde{Q}_1 - \tilde{Q}_2\|(\|\tilde{Q}_1\| + \|\tilde{Q}_2\|)^{-1}$, which also reflects difference in the amplitudes (norms). Here $\langle\cdot\rangle$ denotes averaging over the two-dimensional domain $0 \le \varphi_1, \varphi_2 \le 2\pi$, $\tilde{Q} = Q - \langle Q\rangle$, and norm $\|Q\| = \langle QQ\rangle^{1/2}$.

PRC from coupling function. We decompose the reconstructed functions $Q_{\rm e}(\varphi_{\rm e},\varphi_{\rm r})$ according to Eq. (3). Because the frequency $\omega_{\rm e}$ is unknown, we represent $Q_{\rm e}(\varphi_{\rm e},\varphi_{\rm r}) - \omega_{\rm e} = Z(\varphi_{\rm e})I(\varphi_{\rm r})$ as a product of two functions, considering $\omega_{\rm e}$ as a parameter and searching for minimum of the decomposition error $\|\beta\| = \|Q_{\rm e} - \omega_{\rm e} - ZI\|$; the optimal value is taken for the estimate of the frequency $\omega_{\rm e}$ (see Fig. 5c). Decomposition of a function into a product was performed by means of an iterative scheme (Supplementary Eq. (S5)).

[1] Billman, G. E. Heart rate variability – a historical perspective. *Frontiers in Physiology* **2** (2011).

[2] Winfree, A. T. *The Geometry of Biological Time* (Springer, Berlin, 1980).

[3] Glass, L. & Mackey, M. C. *From Clocks to Chaos: The Rhythms of Life.* (Princeton Univ. Press, Princeton, NJ, 1988).

[4] Glass, L. Synchronization and rhythmic processes in physiology. *Nature* **410**, 277–284 (2001).

[5] Moser, M., Frühwirth, M., Penter, R. & Winker, R. Why life oscillates – from a topographical towards a functional chronobiology. *Cancer Causes Control.* **17**, 591–599 (2006).

[6] Moser, M., Frühwirth, M. & Kenner, T. The symphony of life - importance, interaction and visualization of biological rhythms. *IEEE Eng. Med. Biol.* **27**, 29–37 (2008).

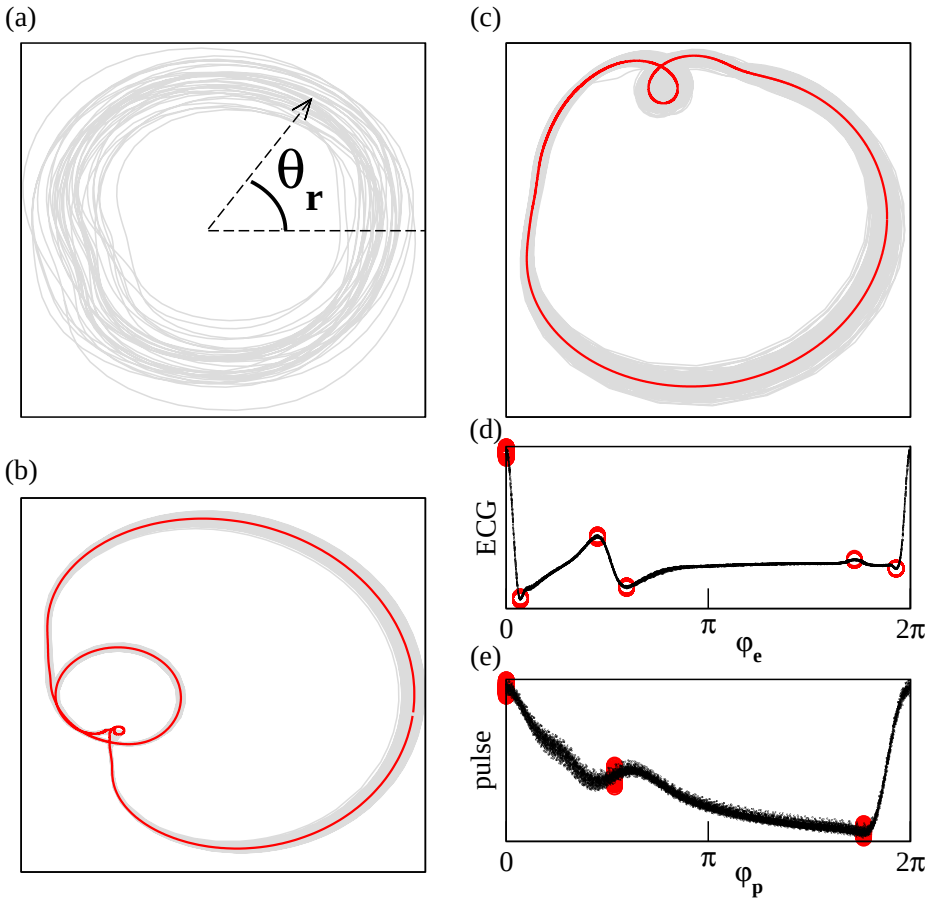

FIG. 8. Phase extraction from the registered data. Two-dimensional embeddings of the registered signals (grey lines) by virtue of the Hilbert transform (x-coordinate: original signal, y-coordinate: its Hilbert transform) for respiration (a) (here also the definition of the protophase is depicted), ECG (b), and arterial pulse (c). Red lines in (b,c) show the average cycles for the ECG and the arterial pulse. Panels (d,e) show marker events within one ECG cycle and arterial pulse cycle, respectively.

[7] Kuramoto, Y. *Chemical Oscillations, Waves and Turbulence* (Springer, Berlin, 1984).

[8] Canavier, C. Phase response curve. *Scholarpedia* **1** (2006).

[9] Perez Velazquez, J. L. *et al.* Phase response curves in the characterization of epileptiform activity. *Phys. Rev. E* **76**, 061912 (2007).

[10] Phoka, E., Cuntz, H., Roth, A. & Häusser, M. A new approach for determining phase response curves reveals that Purkinje cells can act as perfect integrators. *PLoS Comput Biol* **6**, e1000768 (2010).

[11] Schultheiss, N. W., Prinz, A. A. & Butera (Eds.), R. J. *Phase Response Curves in Neuroscience. Theory, Experiment, and Analysis.* Springer, Springer Series in Computational Neuroscience, Vol. 6 (Springer, NY, 2012).

[12] Ikeda, N. Model of bidirectional interaction between myocardial pacemakers based on the phase response curve. *Biological Cybernetics* **43**, 157–167 (1982).

[13] Ikeda, N., Yoshizawa, S. & Sato, T. Difference equation model of ventricular parasystole as an interaction between cardiac pacemakers based on the phase response curve. *Journal of Theoretical Biology* **103**, 439 (1983).

[14] Abramovich-Sivan, S. & Akselrod, S. A single pacemaker cell model based on the phase response curve. *Biological Cybernetics* **79**, 67–76 (1998).

[15] Abramovich-Sivan, S. & Akselrod, S. A pacemaker cell pair model based on the phase response curve. *Biological Cybernetics* **79**, 77–86 (1998).

[16] Abramovich-Sivan, S. & Akselrod, S. Phase response curve based model of the sa node: simulation by two-dimensional array of pacemaker cells with randomly distributed cycle lengths. *Medical and Biological Engineering and Computing* **37**, 482–491 (1999).

[17] Feroah, T. R. *et al.* Effects of spontaneous swallows on breathing in awake goats. *Journal of Applied Physiology* **92**, 1923–1935 (2002).

[18] Khalsa, S. B. S., Jewett, M. E., Cajochen, C. & Czeisler, C. A. A phase response curve to single bright light pulses in human subjects. *J. Physiol.* **549**, 945–952 (2003).

[19] Hilaire, M. A. S. *et al.* Human phase response curve to a 1h pulse of bright white light. *J. Physiol.* **590**, 3035–3045 (2012).

[20] Galán, R. F., Ermentrout, G. B. & Urban, N. N. Efficient estimation of phase-resetting curves in real neurons and its significance for neural-network modeling. *Phys. Rev. Lett.* **94**, 158101 (2005).

[21] Ko, T.-W. & Ermentrout, G. B. Phase-response curves of coupled oscillators. *Phys. Rev. E* **79**, 016211 (2009).

[22] Levnajić, Z. & Pikovsky, A. Phase resetting of collective rhythm in ensembles of oscillators. *Phys. Rev. E* **82**, 056202 (2010).

[23] Galletly, D. C. & Larsen, P. D. Relationship between cardioventilatory coupling and respiratory sinus arrhythmia. *Br J Anaesth.* **80**, 164–8 (1998).

[24] Larsen, P. D. & Galletly, D. C. Cardioventilatory coupling in heart rate variability: the value of standard analytical techniques. *Br J Anaesth.* **87**, 819–26 (2001).

[25] Tzeng, Y. C., Larsen, P. D. & Galletly, D. C. Cardioventilatory coupling in resting human subjects. *Exp Physiol.* **88**, 775–82 (2003).

[26] Schäfer, C., Rosenblum, M. G., Kurths, J. & Abel, H.-H. Heartbeat synchronized with ventilation. *Nature* **392**, 239–240 (1998).

[27] Kralemann, B., Cimponeriu, L., Rosenblum, M., Pikovsky, A. & Mrowka, R. Phase dynamics of coupled oscillators reconstructed from data. *Phys. Rev. E* **77**, 066205 (2008).

[28] McClintock, P. V. E. & Stefanovska, A. Interaction and synchronization in the cardiovascular system. *FNL* **3**, L167–L176 (2003).

[29] Bartsch, R. P., Schumann, A. Y., Kantelhardt, J. W., Penzel, T. & Ivanov, P. C. Phase transitions in physiologic coupling. *PNAS* **109**, 10181–10186 (2012).

[30] Stutte, K. H. & Hildebrandt, G. Untersuchungen über die Koordination von Herzschlag und Atmung. *Pflügers Arch.* **289**, R47 (1966).

[31] Raschke, F. Coordination in the circulatory and respiratory systems. In Rensing, L., an der Heiden, U. & Mackey, M. (eds.) *Temporal Disorder in Human Oscillatory Systems*, vol. 36 of *Springer Series in Synergetics*, 152–158 (Springer-Verlag, Berlin Heidelberg, 1987).

[32] Raschke, F. The respiratory system - features of modulation and coordination. In Haken, H. & Koepchen, H. P. (eds.) *Rhythms in Physiological Systems*, vol. 55 of *Springer Series in Synergetics*, 155 – 164 (Springer-Verlag, Berlin Heidelberg, 1991).

[33] Moser, M. *et al.* Phase and frequency coordination of cardiac-function and respiratory-function. *Biol. Rhythm Res.* **26**, 100–111 (1995).

[34] Mrowka, R., Cimponeriu, L., Patzak, A. & Rosenblum, M. Directionality of coupling of physiological subsystems - age related changes of cardiorespiratory interaction during different sleep stages in babies. *American J. of Physiology Regul. Comp. Integr. Physiol.* **145**, R1395–R1401 (2003).

[35] Mrowka, R., Patzak, A. & Rosenblum, M. G. Qantitative analysis of cardiorespiratory synchronization in infants. *Int. J. of Bifurcation and Chaos* **10**, 2479–2488 (2000).

[36] Stefanovska, A. & Bračič, M. Physics of the human cardiovascular system. *Contemp Phys* **40**, 31–55 (1999).

[37] McGuinness, M., Hong, Y., Galletly, D. C. & Larsen, P. D. Arnold tongues in human cardiorespiratory systems. *Chaos* **14**, 1–6 (2004).

[38] Shiogai, Y., Stefanovska, A. & McClintock, P. V. Nonlinear dynamics of cardiovascular ageing. *Phys Rep.* **488**, 51–110 (2010).

[39] Bahraminasab, A., Ghasemi, F., Stefanovska, A., McClintock, P. V. E. & Kantz, H. Direction of coupling from phases of interacting oscillators: A permutation information approach. *Phys. Rev. Lett.* **100**, 084101 (2008).

[40] Stankovski, T., Duggento, A., McClintock, P. V. E. & Stefanovska, A. Inference of time-evolving coupled dynamical systems in the presence of noise. *Phys. Rev. Lett.* **109**, 024101 (2012).

[41] Blaha, K. A. *et al.* Reconstruction of two-dimensional phase dynamics from experiments on coupled oscillators. *Phys. Rev. E* **84**, 046201 (2011).

[42] Tenreiro, C. Fourier series-based direct plug-in bandwidth selectors for kernel density estimation. *Journal of Nonparametric Statistics* **23**, 533–545 (2011).

[43] Kantz, H. & Schreiber, T. *Nonlinear Time Series Analysis* (Cambridge University Press, Cambridge, 2004). 2nd edition.

[44] Berntson, G. G. *et al.* Heart rate variability: Origins, methods, and interpretive caveats. *Psychophysiology* **34**, 623–648 (1997).

[45] Cysarz, D. *et al.* Oscillations of heart rate and respiration synchronize during poetry recitation. *Am. J. Physiol. Heart Circ. Physiol.* **2872**, H579–H587 (2004).

[46] Strauss-Blasche, G. *et al.* Relative timing of inspiration and expiration affects respiratory sinus arrhythmia. *Clin. Exp. Pharmacol. Physiol.* **27**, 601–606 (2000).

[47] Eckberg, D. L. Point: Counterpoint: Respiratory sinus arrhythmia is due to a central mechanism vs. respiratory sinus arrhythmia is due to the baroreflex mechanism. *J Appl Physiol* **106**, 1740–1742 (2009).

[48] Karemaker, J. M. Last word on point:Counterpoint: Respiratory sinus arrhythmia is due to a central mechanism vs. respiratory sinus arrhythmia is due to the baroreflex mechanism. *J Appl Physiol* **106**, 1750 (2009).

[49] Paulev, P. & Zubieta-Calleja, G. *Medical Physiology And Pathophysiology. Essentials and clinical problems* (Copenhagen Medical Publishers, Copenhagen, 2001). 2nd edition.

[50] Ludwig, C. Beiträge zur Kenntnis des Einflusses der Respirationsbewegung auf den Blutlauf im Aortensystem. *Arch. Anat. Physiol.* **13**, 242–302 (1847).

[51] Moser, M. *et al.* Heart rate variability as a prognostic tool in cardiology. A contribution to the problem from a theoretical point of view. *Circulation* **90**, 1078–1082 (1994).

[52] Cysarz, D. *et al.* Comparison of respiratory rates derived from heart rate variability, ecg amplitude, and nasal/oral airflow. *Ann. Biomed. Eng.* **36**, 2085–2094 (2008).

[53] Bowen, W. P. *Contributions to Medical Research* (University of Michigan, Ann Arbor, 1903).

[54] Garcia III, A. J., Koschnitzky, J. E., Dashevskiy, T. & Ramirez, J.-M. Cardiorespiratory coupling in health and disease. *Autonomic Neuroscience: Basic and Clinical* (2013). In press, published online March 2013.

[55] Florian, G., Stancak, A. & Pfurtscheller, G. Cardiac response induced by voluntary self-paced finger movement. *Int. J. Psychophysiol.* **28**, 273–283 (1998).

[56] Choi, J. & Gutierrez-Osuna, R. Removal of respiratory influences from heart rate variability in stress monitoring. *IEEE Sensors J.* **11**, 2649–2656 (2011).

[57] Katz, A. M. *Physiology of the heart* (Raven Press, NY, 1992). 2nd edition.

[58] Göktepe, S. & Kuhl, E. Computational modeling of cardiac electrophysiology: A novel finite element approach. *Int. J. Num. Meth. Engng.* **79**, 156–178 (2009).

[59] Gallasch, E. *et al.* Instrumentation for assessment of tremor, skin vibrations, and cardiovascular variables in MIR space missions. *IEEE Trans. Biomed. Eng.* **43**, 328–333 (1996).

[60] Gallasch, E., Moser, M., Kozlovskaya, I., Kenner, T. & Noordergraaf, A. Effects of an eight-day space flight on microvibration and physiological tremor. *Amer. J Physiol, Regul Integr Card* **273**, R86–R92 (1997).

ACKNOWLEDGEMENTS

We acknowledge support from the Merz-Stiftung, Berlin and from DFG (FOR 868). We are grateful to I. Semler for providing the drawing used in Fig. 1 after the photo from F. Reil and D. Messerschmidt, and to B. Puswald for writing the data acquisition software and assistance with the measurements. We acknowledge valuable contribution of L. Dogariu (Cimponeriu) at the early stage of this project, and fruitful discussions with R. Mrowka.

AUTHOR CONTRIBUTIONS

MF performed experiments. BK, AP, and MR developed the algorithms and analysed the data. MF, TK, JS, and MM provided physiological interpretation. AP and MR wrote the manuscript, with contribution of all authors. All authors have read and approved the final version of the manuscript.

ADDITIONAL INFORMATION

Corresponding author: MR (mros@uni-potsdam.de)
Supplementary Information accompanies this paper at
`http://www.nature.com/naturecommunications`
Competing financial interests: The authors declare no competing financial interests.

Supplementary Information

Code	Age	Sex	Number of respiration - ECG data sets	Number of respiration - pulse data sets
V01	37	m	2	3
V02	39	f	0	1
V04	39	f	2	0
V06	30	f	1	0
V07	32	m	2	0
V08	39	m	1	4
V09	37	f	1	1
V11	40	m	2	2
V12	27	m	0	2
V14	29	m	2	0
V15	43	f	1	0
V16	40	m	2	1
V17	30	m	2	0
V21	43	m	2	0
V23	28	m	2	4
V24	27	f	2	2
V25	51	f	2	0
	Average age: 36		Total number: 26	Total number: 20

Supplementary Table S1. Summary of the data used. For 17 subjects we have obtained from 1 to 6 data sets of sufficient quality for the subsequent analysis, with totally 26 respiration – ECG bivariate data sets and 20 respiration – arterial pulse sets. The average age of the group is 36, with 7 female and 10 male subjects (average age 38 and 34.5, respectively).

SUPPLEMENTARY METHODS

Measurements and preprocessing.

We performed experiments with 17 healthy subjects and recorded ECG, respiratory flow, and pulse wave. The description of the data sets is summarised in Supplementary Table S1.

Respiratory data. Preprocessing of respiratory time series was performed in the following way: (i) manual correction of artefacts by interpolation, (ii) smoothing by Savitzky-Golay filter of order 1 with the window length 0.75s, and (iii) elimination of slow baseline fluctuations by means of fitting and subtracting Fourier modes with the periods $T = 420$s (total record length), $T/2$, $T/3$,..., T_{min}, where T_{min} corresponds to 4 average respiration periods. An example of the original and preprocessed signals is shown in Supplementary Figure S3.

ECG and arterial pulse data. The signals have been smoothed with the help of the first-order Savitzky-Golay filter with the window length 0.025s (Supplementary Figure S4). Next, slow variation of the baseline was cleansed by fitting and subtracting Fourier modes with the periods $T = 420$s, $T/2$, ..., $T/210$, i.e. slower than 2s. (Notice that the quality of our ECG records is very high and the baseline fluctuations were very small; however, this preprocessing step has been performed for consistency with other records.) Next, in order to reduce the slow amplitude variations of the ECG, we detected the R-peaks, fitted their heights by a 3rd-order polynomial function of time $R(t)$, and divided the ECG signal by $R(t)$. Finally, we normalised the ECG so that its maximal value is one. Arterial pulse signals have been preprocessed in the same way as the ECG signals (Supplementary Figure S5).

PRC from bivariate data: Methods in details

Protophase determination.

Here we describe how to compute the protophases $\theta_{r,e,p}$ for the observables, recorded in our experiments, where we consider the heart and the respiratory cycles as outputs of coupled oscillatory systems approximately obey-

ing Eqs. (1) in the main text. Protophase is an angle variable that parametrises the signal, grows monotonically, but generally not uniformly, in time, and gains 2π at each cycle. Important is that the protophase is not defined from the timing within the cycles of the signal, but shall be related to the state of the oscillatory system, via construction of an embedding. For the respiration we obtain θ_r from a two-dimensional state plane, where one coordinate is the signal $x(t)$ itself and another one is its Hilbert transform $\hat{x}(t)$ (see Fig. 8a in the main text). Here the dynamics on the state plane looks like rotations, and the protophase is identified with the polar angle with respect to some origin, i.e. $\theta = \arctan(\hat{x}/x)$. For complex waveforms like the ECG signal the construction of the protophase is highly non-trivial. Here we use a novel three-step technique; the first two steps are described in the main text. In the third step we introduce the protophase θ_e, projecting the analytic signal $z(t)$ onto the average cycle with the help of an optimisation strategy, described below.

Cardiac protophase via projection on the average cycle.

We have to assign protophases to all points of the trajectory $z(t)$. For the points on the cycle itself we simply take $\theta_e = \psi$. In order to ascribe the protophase to the points in the neighbourhood of the average cycle z_{ac}, we project each point of the complex time series $z(t)$ onto the average cycle. Namely, we search for the point $z_{ac}(\psi_0)$ on the average cycle, which has the minimal Euclidean distance to $z(t)$, i.e. we find $\min_{\psi_0}\left\{|z(t) - z_{ac}(\psi_0)|^2\right\}$, and assign $\theta_e(t) = \psi_0$.

Here, the following problem has to be solved. In the time interval between the minimum after the T-wave and the P-wave, i.e. between the 4th and 5th markers (cf. Fig. 8d in the main text), the ECG signal is nearly constant and therefore is dominated by fluctuations: the variation of the signal due to the variation of protophase is smaller than its variation due to noise or amplitude dynamics. Hence, within this region the signal contains practically no information about the protophase of the system. To overcome this difficulty, we added another term to the minimisation condition, which now reads

$$\min_{\psi_0}\left\{|(z(t) - z_{ac}(\psi_0)|^2 + \alpha\left|e^{i\Psi(t)} - e^{i\psi_0}\right|^2\right\}\ , \quad \text{(S1)}$$

where the term $\alpha\left|e^{i\Psi(t)} - e^{i\psi_0}\right|^2$ quantifies the discrepancy between the preliminary estimate of the protophase $\Psi(t)$ and the point ψ_0 on the average cycle z_{ac}. This term plays the role of a cost function, forcing the minimisation procedure to look for solutions in the vicinity of $\Psi(t)$. The minimisation is achieved in a trade-off between minimising the distance between the point $z(t)$ and the average cycle $z_{ac}(\psi)$, i.e. $|(z(t) - z_{ac}(\psi_0)|$, and minimising the deviation of $\theta_e(t) = \psi_0$ from the initial estimate $\Psi(t)$, where the relative weight of both terms is determined by the factor α. If $\alpha = 0$, the solution is solely determined by the distance between signal an average cycle; for large values of α the minimisation will reproduce the values of the preliminary estimate $\Psi(t)$. Furthermore, the result of the trade-off depends on the time structure of the signal. In the regions of fast dynamics, where $\dfrac{\partial z}{\partial \psi}$ is large, the term $|z(t) - z_{ac}(\psi_0)|^2$ strongly contributes to the minimisation, while in regions with a nearly flat signal, its contribution is negligible. On the contrary, here the term describing the deviation from the initial estimate will dominate. Since the trade-off also depends on the absolute values of the signal $z(t)$, the signal is always normalised to $\max[z(t)] = 1$. Practically, the minimisation procedure is performed with the MATLAB (The Mathworks, Natick, MA) function *fminbnd*.

The optimal value of the parameter α has to be estimated empirically for the particular form of the signal, noise level, and baseline fluctuation. We suggest the following procedure. In the first step we simulate the phase model

$$\begin{aligned} \dot{\varphi}_e^{test} &= \omega_e + \textstyle\sum_{n,m\neq 0} F_{n,m} e^{(n\varphi_e^{test} + m\varphi_r^{test})}\ , \\ \dot{\varphi}_r^{test} &= \omega_r\ , \end{aligned} \quad \text{(S2)}$$

in order to generate test phase time series φ_e^{test} and φ_e^{test}, where the natural frequencies are $\omega_r = 2$ and $\omega_e = 2\pi$. Here $F_{n,m}$ are Fourier coefficients of the test coupling function; the non-zero coefficients are: $F_{0,\pm 1} = 0.05$, $F_{\pm k,\mp 1} = 0.1$, with $k = 1, 2, 3, 4$. Next, we generate a test ECG signal $\mathcal{E}^{test} = z_{ac}(\varphi_e^{test})$, using the average cycle, obtained from the ECG to be analysed. To imitate the real ECG signals, we added some noise and amplitude variations. In order to simulate the effect of respiration, we introduced amplitude variations which are periodic in φ_r^{test}. This was achieved with the help of transformation

$$\frac{\mathcal{E}^{test}(t)}{[1 + 0.02\cos[\phi_r^{test}(t)]]^2} + \eta(t) \to \mathcal{E}^{test}(t)\ , \quad \text{(S3)}$$

where $\eta(t)$ is Gaussian uncorrelated noise with standard deviation $\sigma = 0.001 \cdot \max(\mathcal{E}^{test})$. An example of the test signal $\mathcal{E}^{test}$ is shown in Supplementary Figure S6. Next, from the contaminated test time series we reconstructed phase models Q_α for different values of α. These reconstructed models were compared to the known original phase model Q^{test} by means of the correlation $\rho(Q_\alpha, Q^{test})$ and of the difference measure $\eta(Q_\alpha, Q^{test})$, see Supplementary Figure S7. The maximal respectively minimal values are found for $\alpha = 0.15$. Therefore, the value $\alpha = 0.15$ appears to be the optimal choice for the imitated signals. Since the real ECG signals are not as clean as the simulated ones and since this optimal value is very close to the border of quality breakdown, we choose a value in the saturation region, namely $\alpha = 0.5$ for real

ECG data computations. As can be seen from Supplementary Figure S7, this choice reduces the correlation by 2%, but makes the processing more reliable. For pulse date we used the same procedure leading to an optimal value of $\alpha = 0.8$.

PRC from coupling function.

We decompose the reconstructed functions $Q_e(\varphi_e, \varphi_r)$ according to

$$Q_e(\varphi_e, \varphi_r) = \omega_e + Z(\varphi_e)I(\varphi_r) + \beta(\varphi_e, \varphi_r) \ , \qquad \text{(S4)}$$

with the residual β characterising the quality of the decomposition. Because the frequency ω_e is unknown, we represent $Q_e(\varphi_e, \varphi_r) - \omega_e$ as a product of two functions, considering ω_e as a parameter and searching for minimum of the decomposition error $\|\beta\| = \|Q_e - \omega_e - ZI\|$; the optimal value is taken for the estimate of the frequency ω_e. Here $\|\beta\| = \sqrt{\langle\beta^2\rangle}$ denotes the norm of the function, whereas $\langle\cdot\rangle$ denotes averaging of a function over the two-dimensional domain $0 \le \varphi_1, \varphi_2 \le 2\pi$. Decomposition of a function into a product $S(x, y) = f(x)g(y)$ was performed by means of the following iterative scheme:

$$\begin{aligned} f_{n+1}(x) &= \frac{\int_0^{2\pi} S(x,y)g_n(y)dy}{\int_0^{2\pi} g_n^2(y)dy} \ , \\ g_{n+1} &= \frac{\int_0^{2\pi} S(x,y)f_{n+1}dx}{\int_0^{2\pi} f_{n+1}^2(x)dx} \ , \end{aligned} \qquad \text{(S5)}$$

with the initial function taken as $g_0(y) = S(\bar{x}, y)$, where $S(\bar{x}, \bar{y}) = \max_{x,y} S(x, y)$. Numerical tests show that the procedure converges very fast, namely at most 5 iterations are required.

PRC: additional discussion

Normalisation. The decomposition $Q(\varphi_e, \varphi_r) = \omega + Z(\varphi_e)I(\varphi_r)$ contains a free parameter which cannot be determined from the coupling function Q, namely the relative scaling of functions Z and I: rescaling $Z \to bZ$, $I \to b^{-1}I$ yields the same Q. Thus, if no further information is available, only the shape of the PRC $Z(\varphi_h)$ can be determined, but not its amplitude. In our presentation in Fig. 5 in the main text we made the norms of Z and I equal. Another, quite natural option is to assume that the norm of I is roughly proportional to the norm (standard deviation) of the respiratory signal. Here we adopt this, although in our measurements the relation between the intensity of respiration and the amplitude of the measured quantity (thermistor output) is rather weak, as it is distorted by variations of the environment temperature and other factors. In this normalisation the PRC is measured in units of $\sec^{-1}[\mathrm{r}]^{-1}$ where [r] is the dimension of the respiratory signal (in our case mV). In Supplementary Figure S2, together with functions Z and I obtained via decomposition of all obtained coupling functions Q_e, we also present the averaged functions, obtained either by (i) averaging all functions Z and all functions I or (ii) by decomposing the averaged coupling function, shown in Fig. 2e in the main text. It is important to emphasise that averaged functions Z and I obtained via different normalisation techniques are very close (cf. Fig. 5 in the main text).

PRC from Q_p functions. PRC and effective forcing obtained from arterial pulse – respiration functions are shown in Supplementary Figure S1, to be compared with Fig. 3 in the main text and with Supplementary Figure S2. It can be seen that the effective force is nearly the same, as the one obtained from Q_r functions. The PRCs qualitatively agree with those obtained from ECG, although the refractory period is not so pronounced.

Supplementary Figures

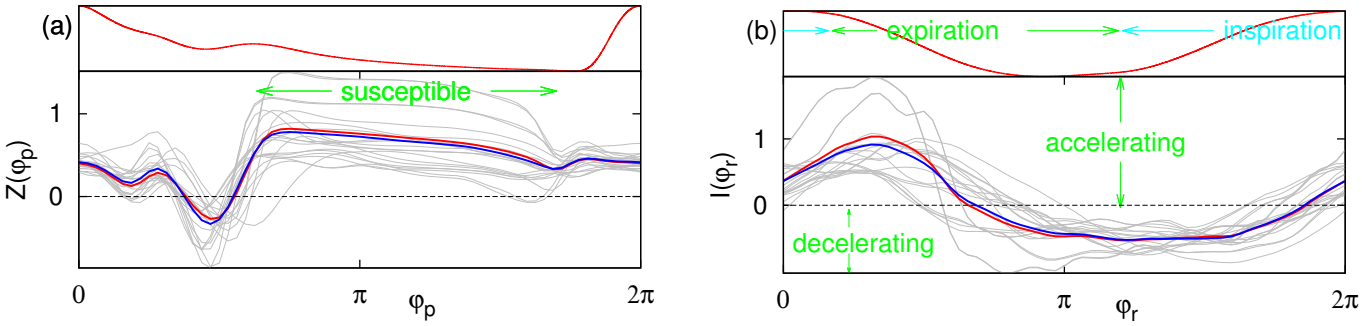

Supplementary Figure S1. Individual PRCs Z (a) and effective forcing I (b) for all pulse-based coupling functions. In both panels blue lines show the average over all individual (grey) curves. Red curves are obtained by decomposition of the averaged coupling function, shown in Fig. 2f in the main text. Small panels on top of (a) and (b) show for comparison the average pulse and respiratory cycles as functions of their phase.

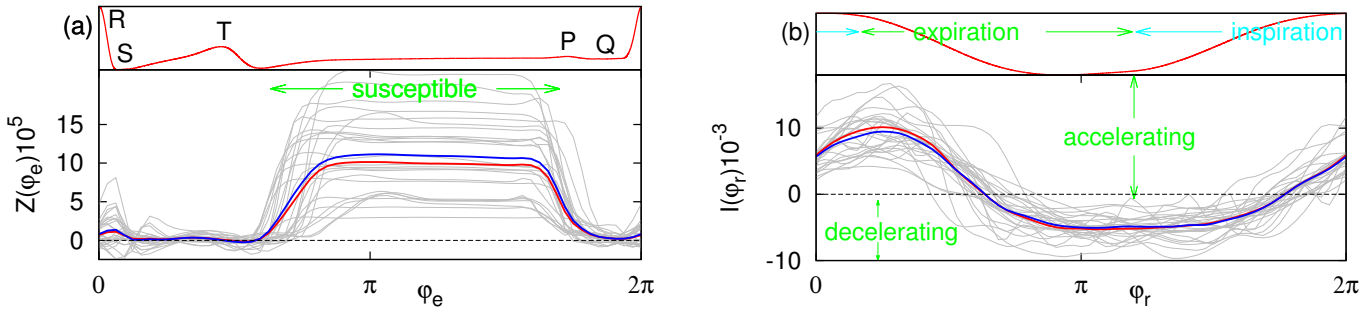

Supplementary Figure S2. Individual PRCs Z (a) and effective forcing I (b) for all ECG-based coupling functions, obtained via another normalisation. In both panels blue lines show the average over all individual (grey) curves. Red curves are obtained by decomposition of the averaged coupling function, shown in Fig. 2e in the main text. Normalisation used here is explained in the text. Small panels on top of (a) and (b) show for comparison the average ECG cycle and the average respiratory cycle as functions of their phase.

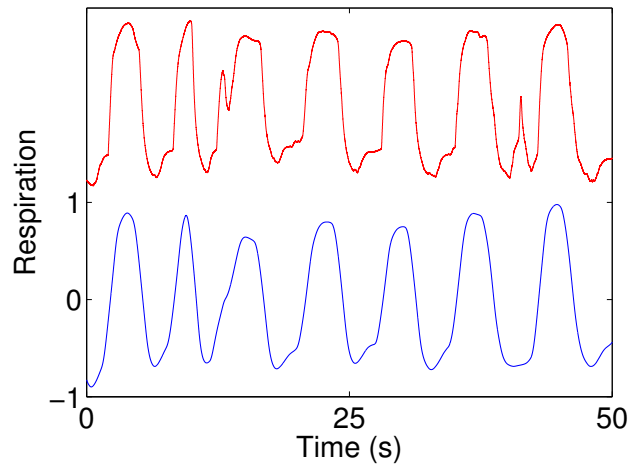

Supplementary Figure S3. Illustration of the respiratory data smoothing. Original signal is shown in red, smoothed signal is shown in blue. Two artefacts at $\approx$ 13s and $\approx$ 41s were manually corrected by interpolation. The signals (arbitrary units) are shifted vertically for better visibility.

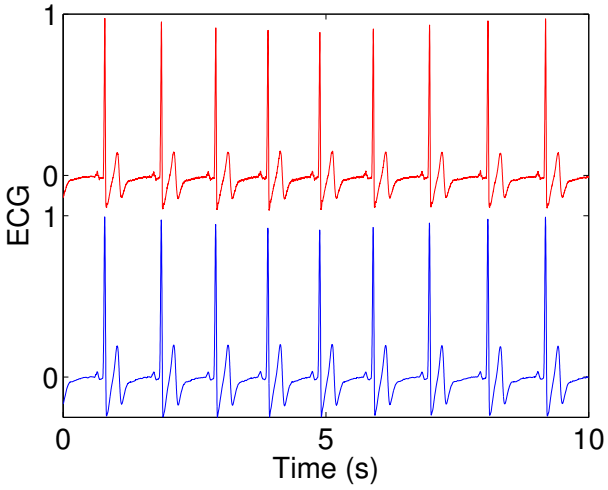

Supplementary Figure S4. Illustration of the ECG smoothing. Original ECG is shown in red, preprocessed signal is shown in blue. The signals (arbitrary units) are shifted vertically for better visibility.

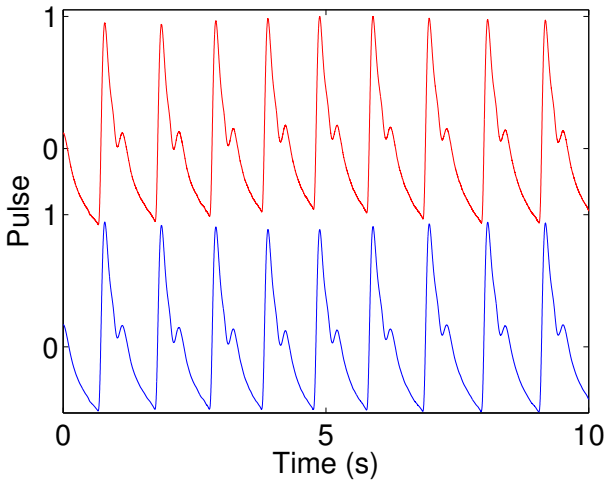

Supplementary Figure S5. Illustration of the arterial pulse smoothing. Original signal is shown in red, amplitude adjusted and smoothed arterial pulse is shown in blue. The signals (arbitrary units) are shifted vertically for better visibility.

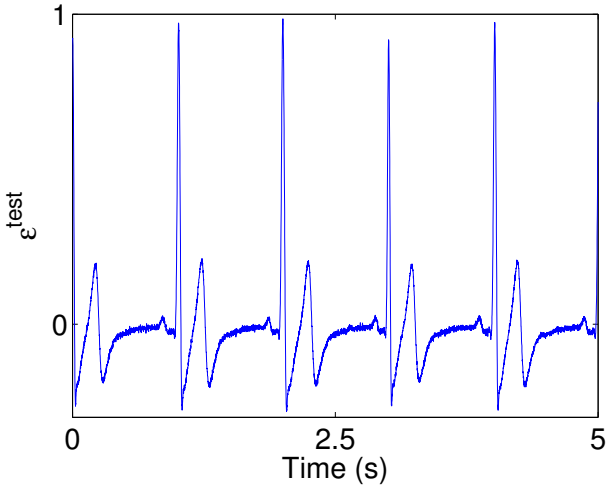

Supplementary Figure S6. The artificial ECG test signal $\mathcal{E}^{test}$ used for the optimisation procedure.

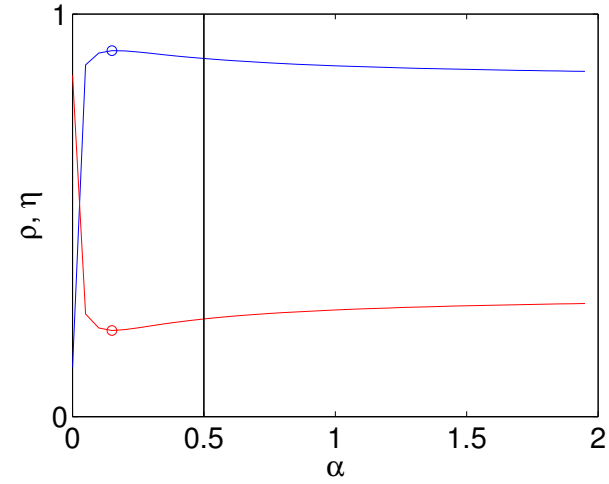

Supplementary Figure S7. Optimisation of the average cycle technique with the help of artificial data. The correlation, $\rho(Q_\alpha, Q^{test})$ (blue), and the difference measure, $\eta(Q_\alpha, Q^{test})$ (red), as functions of the optimisation parameter α, for the ECG – respiration data. The maximal respectively minimal values are found for $\alpha = 0.15$ and marked by circles. The value $\alpha = 0.5$ used for the analysis is marked by vertical line.